The Astrophysical Journal Supplement Series, 242:9 (12pp), 2019 May https://doi.org/10.3847/1538-4365/ab17e1

Collision and Radiative Rates for Infrared to Extreme Ultraviolet Lines of S III

S. S. Tayal[1], O. Zatsarinny[2], and A. M. Sossah[3]
[1] Department of Physics, Clark Atlanta University, Atlanta, GA 30314, USA; stayal@cau.edu
[2] Department of Physics and Astronomy, Drake University, Des Moines, IA 50311, USA; oleg.zatsarinny@drake.edu
[3] Department of Physics, Kennesaw State University, Kennesaw, GA 30144, USA; asossah@kennesaw.edu
Received 2019 January 7; revised 2019 March 20; accepted 2019 March 23; published 2019 May 21

Abstract

Electron excitation collision strengths for a wide range of transitions giving rise to infrared, optical, ultraviolet, and extreme ultraviolet lines of S III have been calculated using the *B*-spline Breit–Pauli *R*-matrix method. The term-dependent non-orthogonal orbitals have been employed for the accurate representation of target wave functions and the electron plus S III target scattering system. The multiconfiguration Hartree–Fock method has been utilized for the calculation of 198 S III fine-structure level energies belonging to the $3s^23p^2$, $3s3p^3$, $3p^4$, $3s^23p3d$, $3s^23p4s$, $4p$, $4d$, $4f$, $3s^23p5s$, $5p$, $5d$, $3s^23p6s$, $3s3p^23d$, $3s3p^24s$, $4p$, $4d$, $4f$, and $3s3p^25s$ configurations. The transition probabilities between fine-structure levels have also been calculated and compared with available other calculations. The close-coupling expansion includes these 198 fine-structure levels of S III in the electron collision calculations. The effective collision strengths are calculated at electron temperatures in the range of 10^3–10^6 K for all possible transitions between the 198 fine-structure levels. The present calculation includes a larger number of levels in the close-coupling expansion and improved target description than previous calculations and should be useful for the analysis of measured spectra from various astrophysical objects. Comparison with other calculations is used to assess likely uncertainties in the existing collision and radiative rates for S III. The collision and radiative rates are estimated to be accurate to about 20% or better for most main transitions of astrophysical importance.

Key words: atomic data – atomic processes – H II regions – planetary systems – plasmas – scattering

Supporting material: machine-readable tables

1. Introduction

In recent years, a number of S III emission features have been observed in the spectral regions from infrared (IR) to extreme ultraviolet (EUV) from a broad range of astrophysical objects. The S III lines may carry important information about physical conditions in the various H II regions, planetary atmospheres, and stellar objects. The S III far-IR emission lines arise due to transitions between the fine-structure levels of the ground $3s^23p^2$ ^3P term and have been observed from a number of extragalactic H II regions with the *Spitzer Space Telescope* (Rubin et al. 2008). The S III far-IR fine-structure lines have also been observed in Seyfert galaxies with the Photoconductor Array Camera and Spectrometer from *Herschel* (Spinoglio et al. 2015). Different emission lines in the same galaxy can arise from physically different components in the galaxy. The [S III] 33.5 μm/18.7 μm line ratio can provide a good density diagnostic for low-density H II regions. The neon to sulfur abundance ratios can be used as a useful metallicity tracer of extragalactic H II regions. The far-IR fine-structure line ratios from *Spitzer* can be used to separate starbursts and active galactic nuclei. In addition to the IR lines, S III lines in the ultraviolet (UV), far-ultraviolet (FUV), and EUV wavelength regions offer good density and temperature diagnostics. The EUV emission lines arise due to transitions between the multiplets $3s^23p^2$ ^3P–$3s^23p4d$ $^3P^o$ and $^3D^o$ in the 480.53–486.14 Å wavelength region. The ratios involving lines within the same multiplet $3s^23p^2$ ^3P–$3s3p^3$ $^3P^o$ provide reliable density diagnostics. The S III $\lambda1015/\lambda1012$ line ratio is electron density sensitive in the density range of 1000–3000 cm^{-3}. The intercombination lines due to the $3s^23p^2$ $^3P_{1,2}$–$3s3p^3$ $^5S^o_2$ transitions in S III at 1713.1 and 1729 Å also offer useful diagnostics. The intensity ratios of S III lines of the $3s^23p^2$ ^3P–$3s3p^3$ $^3D^o$ multiplet to the $3s^23p^2$ ^3P–$3s3p^3$ $^5S^o$ lines are used to infer the electron temperature. The S III lines belonging to the $3s^23p^2$ ^1D–$3s^23p3d$ $^1D^o$ (1077.15 Å) and $3s^23p^2$ ^3P–$3s3p^3$ $^3P^o$ multiplets in the wavelength range of 1012.50–1021.33 Å also provide good electron temperature diagnostic in the range of 70,000–100,000 K. Mendoza & Bautista (2014) and Binette et al. (2012) inferred that T_e(O III) < T_e(S III) in galactic and extragalactic H II regions from the O III and S III UV line ratios. Several UV and EUV emission lines of S III have been observed in Io plasma torus spectra (Feldman et al. 2004; Hall et al. 1994). Some prominent S III emission lines have also been detected in the spectra of the solar quiet region (Curdt et al. 2004).

The uncertainties in transition probabilities and electron excitation collision rates can be a major source of error in S III spectral modeling for determining the electron density, temperature, and chemical abundance. Many times it is difficult to assess the uncertainties of atomic data as the computational approaches rely on several approximations. The previous available electron excitation collision and emission transition rate calculations of increasing sizes include Galavís et al. (1995), Tayal (1997a, 1997b), Tayal & Gupta (1999), Froese Fischer et al. (2006), Hudson et al. (2012), and Grieve et al. (2014). Galavís et al. (1995) and Tayal & Gupta (1999) performed Russell-Saunders (LS)-coupling *R*-matrix calculations and presented effective collision strengths for fine-structure levels determined by transforming LS reactance matrices into pair coupling. Hudson et al. (2012) and Grieve et al. (2014) considered S III 53 fine-structure levels of the $3s^23p^2$, $3s3p^3$, $3s^23p3d$, $4s$, $4p$, and $4d$ configurations using the RMATRIX II plus FINE95 (Burke et al. 1994) computer codes. Hudson et al. (2012) presented effective collision strengths only for the forbidden transitions among the levels of $3s^23p^2$ ground configurations that give rise to IR and optical lines. Later, Grieve et al. (2014) extended the work of Hudson et al. (2012) for transitions to excited levels of other

configurations included in their calculations by adding results for higher partial waves up to $2J = 25$ plus a top-up procedure. The 53-state RMATRIX II plus FINE95 calculations show significant discrepancies with the calculation of Tayal & Gupta (1999) for several transitions, especially for the transitions among the $3s^23p^2$ $^3P_{0,1,2}$ levels and transitions involving levels of the $3s^23p4d$ configuration. Hudson et al. (2012) and Grieve et al. (2014) discussed the causes of these discrepancies. Briefly, Tayal & Gupta (1999) inadvertently omitted the energy region below ~0.1 Ryd from the calculation of collision strengths that have significant impact on the effective collision strengths for transitions among the fine-structure levels $3s^23p^2$ $^3P_{0,1,2}$ at lower temperatures. Tayal & Gupta (1999) also used a coarse energy mesh and thus may have omitted some resonances and neglected $3s^23p4d$ $^3F_{2,3,4}$ levels from the close-coupling expansion because of limited computer resources available at that time. Tayal (1997b) calculated oscillator strengths for allowed (E1) transitions between the 49 fine-structure levels using the computer code CIV3 (Hibbert 1975; Glass & Hibbert 1978) with 13 orthogonal orbitals and major one-electron and two-electron excitations from the main configurations. Tayal (1997b) used the Breit–Pauli approach and included one-body and two-body Breit–Pauli operators in the calculation of transition rates. Froese Fischer et al. (2006) presented energy levels, lifetimes, and transition probabilities using the multiconfiguration Hartree–Fock (MCHF) method (Froese Fischer 2007).

In the present work, our objective is to revisit the S III calculations of transition probabilities and electron excitation collision strengths using highly accurate target wave functions and by including fine-structure effects through the Breit–Pauli Hamiltonian. We present more elaborate and accurate calculations for IR to EUV lines useful for diagnostic calculations of a gaseous nebular, Io plasma torus, and solar atmosphere. We performed a fairly large-scale close-coupling calculation by including 198 fine-structure levels of S III terms belonging to the $3s^23p^2$, $3s3p^3$, $3p^4$, $3s^23p3d$, $3s^23p4s$, $4p$, $4d$, $4f$, $3s^23p5s$, $5p$, $5d$, $3s^23p6s$, $3s3p^2(^3P)3d$, $3s3p^2(^1D)3d$, $3s3p^2(^1S)3d$, $3s^23p5s$, $3s3p^2(^3P)4s$, $4p$, $4d$, $4f$, $3s3p^2(^1D)4s$, $3s3p^2(^1S)4s$, and $3s3p^2(^3P)5s$ configurations. The larger number of target levels in the close-coupling expansions is more likely to provide converged collision strengths for the lines of astrophysical importance. We used *B*-spline Breit–Pauli *R*-matrix (BSR) code (Zatsarinny 2006) in the scattering calculations and included fine-structure effects in the close-coupling expansions directly. The flexible term-dependent non-orthogonal orbitals used in the present work provides a more accurate description of the target and scattering functions than the orthogonal orbitals used in the previous collision calculations. The target levels energies in the scattering calculation were adjusted to experimental values where available. Our calculation should allow inclusion of all important resonances with their correct positions and magnitudes, especially close to thresholds important for diagnostics of low temperature astrophysical plasmas. We present transition probabilities and collision strengths for transitions between fine-structure levels, and our calculations should allow a more complete evaluation of uncertainties in the existing S III data sets.

2. Computational Methods

2.1. Target Wave Function Calculations

In the present work, we used the MCHF code of Froese Fischer (2007) in combination with our configuration-interaction (CI) code with non-orthogonal orbitals to generate the target wave functions. First, the core $1s$, $2s$, and $2p$ orbitals were obtained from a Hartree–Fock calculation of the ground state. These orbitals were kept fixed in the subsequent generation of valence spectroscopic orbitals. The $3s$, $3p$, $3d$, $4s$, $4p$, $4d$, $4f$, $5s$, $5p$, $5d$, and $6s$ valence orbitals were generated specifically for each main configuration by choosing various terms of even and odd parities. The term dependence of the $3s$ and $3p$ radial functions is important for the $3s3p^3$ $^3P^o$, $^1P^o$, $^3S^o$, $^1D^o$, $^5S^o$, $3s^23p3s$ $^3P^o$, $^1P^o$, and $3p^4$ ^1D, ^1S states. There is very strong mixing between the $^3P^o$ terms of the $3s^23p3d$ and $3s^23p4s$ configurations, which makes their unambiguous identification difficult based on the dominant eigenvectors. The terms of $3s^23p3d$ configuration also have strong interactions with the $3s3p^3$, $3p^33d$, $4d$, $5d$, and $3s3p3d^2$ configurations. For example, the eigenvector composition for the $3s^23p3d$ $^3P^o$ state is $0.669(3s^23p3d)+0.628(3s^23p4s)+0.283(3s3p^3)+0.102(3p^33d)$, and for the $3s^23p4s$ $^3P^o$ state, the composition is $0.739(3s^23p4s)+0.555(3s^23p3d)+0.277(3s3p^3)+0.123(3p^34s)$. Similarly, the composition of the $3s3p^2(^2D)3d$ ^3P state is $0.504(3s3p^23d)+0.438(3s3p^24s)+0.432(3p^4)$. We chose four sets of orthogonal correlation orbitals to account for important correlation effects. The correlation orbitals $6s$, $6p$, $6d$, and $6f$; and $7s$, $7p$, $7d$, and $7f$ were generated on the ground $3s^23p^2$ ^3P and on the $3s^23p4p$ ^3D states, respectively, and were used for all even parity states. The $8s$, $8p$, $8d$, and $8f$; and $9s$, $9p$, $9d$, and $9f$ correlation orbitals were optimized on the $3s3p^3{}^3D^o$ and $3s^23p3d$ $^3P^o$ states, respectively, and were then used for all odd parity states. It may be noted that the principle quantum number, n, in the correlated orbitals is not related to nodes and serves to represent different subsets of orbitals. We used a total of 125 spectroscopic and correlation orbitals to describe 198 target fine-structure levels. The term dependence of the valence orbitals was noticeable for accurate calculation of term energies. The final configuration expansions contain all of the most important single and double excitations from the valence orbitals of the main configurations. Inclusion of all possible promotions leads to very large configuration expansions. Therefore, we attempted to include most important correlation effects for the target states to keep the target expansions of manageable sizes, which are appropriate for the scattering calculations. We chose cut-off parameters in the range from 0.020 to 0.025 for the different terms due to different convergence patterns. We managed to include 712 configurations to represent all 92 LS target terms with this scheme. These 92 LS terms give rise to a total of 198 fine-structure levels.

The *J*-dependent atomic state functions are written as a sum over different LS values that couple to give the total angular momentum J. We determined J-dependent target states by diagonalizing the Breit–Pauli Hamiltonian on the basis of multiconfiguration LS wave functions (Zatsarinny & Froese Fischer 2000). The target expansion for total angular momentum J and parity π has the form

$$\Psi^{J\pi} = \sum_{\alpha LS} C(J\pi;\, \alpha LS\pi)\Phi^{\alpha LS\pi}. \quad (1)$$

We included all one-electron Breit–Pauli operators and spin–other-orbit and spin–spin two-body operators in our calculations of transition probabilities. The functions $\Phi^{\alpha LS\pi}$ in the above equation are the multi-configurational expansions from the LS calculations, and no cut-off factor has been applied at this stage. The diagonalization of the Breit–Pauli atomic

Table 1
Comparison of Energy Levels (Ry) and Lifetimes (*ns*) of Excited Levels of S III

Index–CFG–LSJ	Excitation Energy					Lifetime	
	Present	Exp.	CFF	TG	AEM	Present	CFF
1 $3s^23p^2\ ^3P_0$	0.00000	0.00000	0.00000	0.00000	0.00000		
2 $3s^23p^2\ ^3P_1$	0.00237	0.00272	0.00243	0.00230	0.00272	3.29(+12)	2.93(+12)
3 $3s^23p^2\ ^3P_2$	0.00672	0.00759	0.00675	0.00660	0.00765	7.04(+11)	6.99(+11)
4 $3s^23p^2\ ^1D_2$	0.10896	0.10318	0.10466	0.12520		1.29(+10)	1.41(+10)
5 $3s^23p^2\ ^1S_0$	0.25063	0.24751	0.25041	0.26690		3.34(+8)	3.47(+8)
6 $3s3p^3(^4S)\ ^5S_2^o$	0.53330	0.53466	0.52313	0.50420		5.78(+4)	5.96(+4)
7 $3s3p^3(^2D)\ ^3D_1^o$	0.76486	0.76564	0.75930	0.75640	0.78570	1.46(+1)	1.46(+1)
8 $3s3p^3(^2D)\ ^3D_2^o$	0.76520	0.76589	0.75953	0.75650	0.78568	1.47(+1)	1.48(+1)
9 $3s3p^3(^2D)\ ^3D_3^o$	0.76582	0.76637	0.75994	0.75690	0.78559	1.50(+1)	1.50(+1)
10 $3s3p^3(^2P)\ ^3P_2^o$	0.89989	0.89983	0.89624	0.88220	0.90949	3.50	3.55
11 $3s3p^3(^2P)\ ^3P_1^o$	0.90018	0.90002	0.89652	0.88220	0.90952	3.40	3.47
12 $3s3p^3(^2P)\ ^3P_0^o$	0.90027	0.90008	0.89659	0.88210	0.90956	3.36	3.43
13 $3s^23p3d\ ^1D_2^o$	0.94280	0.94917	0.94728	0.95550	0.92499	7.41	7.35
14 $3s^23p3d\ ^3F_2^o$	1.10503	1.11283	1.11375	1.22810	1.14174	1.14(+3)	1.29(+3)
15 $3s^23p3d\ ^3F_3^o$	1.10744	1.11543	1.11611	1.12520	1.14407	8.15(+2)	9.86(+2)
16 $3s^23p3d\ ^3F_4^o$	1.11073	1.11902	1.11935	1.12840	1.14718		
17 $3s3p^3(^2P)\ ^1P_1^o$	1.25721	1.24701	1.25750	1.28690	1.26265	1.55(−1)	1.64(−1)
18 $3s3p^3(^4S)\ ^3S_1^o$	1.26343	1.25815	1.27501	1.29370	1.31493	7.42(−2)	7.42(−2)
19 $3s^23p3d\ ^3P_0^o$	1.30653	1.30400	1.30373	1.34760	1.30418	1.02(−1)	9.80(−2)
20 $3s^23p3d\ ^3P_1^o$	1.30734	1.30418	1.34760	1.30272		9.91(−2)	9.55(−2)
21 $3s^23p3d\ ^3P_2^o$	1.30895	1.30425	1.30546	1.34870	1.29986	9.29(−2)	9.09(−2)
22 $3s^23p4s\ ^3P_0^o$	1.34683	1.33680	1.34211	1.31010	1.35889	5.10(−1)	7.28(−1)
23 $3s^23p4s\ ^3P_1^o$	1.34737	1.33717	1.34197	1.30910	1.36143	4.23(−1)	6.55(−1)
24 $3s^23p4s\ ^3P_2^o$	1.34760	1.34090	1.34461	1.31170	1.36652	6.68(−1)	9.62(−1)
25 $3s^23p3d\ ^3D_1^o$	1.35127	1.34459	1.35217	1.37070	1.32378	6.98(−2)	7.06(−2)
26 $3s^23p3d\ ^3D_2^o$	1.35251	1.34587	1.35322	1.37170	1.32447	7.12(−2)	7.19(−2)
27 $3s^23p3d\ ^3D_3^o$	1.35265	1.34636	1.35390	1.37250	1.32549	6.87(−2)	6.96(−2)
28 $3s^23p4s\ ^1P_1^o$	1.33969	1.35231	1.35192	1.37400	1.35729	4.14(−1)	3.64(−1)
29 $3s3p^3(^2D)\ ^1D_2^o$	1.40215	1.38493	1.39896	1.42390	1.39100	7.35(−2)	7.42(−2)
30 $3s^23p3d\ ^1F_3^o$	1.45436	1.43625	1.44380	1.48960	1.40778	7.21(−2)	7.18(−2)
31 $3s^23p3d\ ^1P_1^o$	1.52306	1.49576	1.52180	1.55450	1.42424	8.16(−2)	8.16(−2)
32 $3s^23p4p\ ^1P_1$	1.53057	1.52686	1.52555	1.53890	1.47752	2.48	2.50
33 $3s^23p4p\ ^3D_1$	1.55295	1.54707	1.54580	1.57540	1.58419	2.09	2.06
34 $3s^23p4p\ ^3D_2$	1.55546	1.54978	1.54824	1.57800	1.58702	2.08	2.04
35 $3s^23p4p\ ^3D_3$	1.56027	1.55508	1.55288	1.58390	1.59127	2.07	2.03
36 $3s^23p4p\ ^3P_0$	1.57503	1.57315	1.57046	1.57680	1.61717	2.09	2.06
37 $3s^23p4p\ ^3P_1$	1.57631	1.57455	1.57171	1.57870	1.61858	2.09	2.06
38 $3s^23p4p\ ^3P_2$	1.57946	1.57825	1.57491	1.58240	1.62140	2.12	2.09
39 $3s^23p4p\ ^3S_1$	1.58832	1.58595	1.58322	1.58610	1.61990	2.01	1.96
40 $3s^23p4p\ ^1D_2$	1.62187	1.61280	1.61003	1.65320	1.62192	2.90	2.94
41 $3s3p^2(^4P)3d\ ^3P_2$	1.66373		1.65837			2.03	2.10
42 $3s^23p4p\ ^1S_0$	1.67148	1.66542	1.66426	1.67710	1.69092	2.21	2.15
43 $3s3p^2(^4P)3d\ ^3P_1$	1.66676		1.66177			2.05	2.12
44 $3s3p^2(^4P)3d\ ^3P_0$	1.66817		1.66332			2.07	2.17
45 $3s3p^2(^4P)3d\ ^5F_1$	1.68006					9.90(+3)	
46 $3s3p^2(^4P)3d\ ^5F_2$	1.68085					1.16(+4)	
47 $3s3p^2(^4P)3d\ ^5F_3$	1.68206					1.56(+4)	
48 $3s3p^2(^4P)3d\ ^5F_4$	1.68369					2.60(+4)	
49 $3s3p^2(^4P)3d\ ^5F_5$	1.68575					9.04(+4)	
50 $3s3p^2(^4P)3d\ ^5D_0$	1.73607					1.44(+3)	
51 $3s3p^2(^4P)3d\ ^5D_1$	1.73628					7.91(+2)	
52 $3s3p^2(^4P)3d\ ^5D_2$	1.73670					4.89(+2)	
53 $3s3p^2(^4P)3d\ ^5D_3$	1.73734					4.70(+2)	
54 $3s3p^2(^4P)3d\ ^5D_4$	1.73820					2.89(+4)	
55 $3p^4\ ^1D_2$	1.75041					2.83	
56 $3s3p^2(^2D)3d\ ^3F_2$	1.82314					1.76(+1)	
57 $3s3p^2(^2D)3d\ ^3F_3$	1.82458					1.86(+1)	
58 $3s3p^2(^2D)3d\ ^3F_4$	1.82654					2.02(+1)	

Table 1
(Continued)

Index–CFG–LSJ	Excitation Energy					Lifetime	
	Present	Exp.	CFF	TG	AEM	Present	CFF
59 $3s^23p4d\ ^3F_2^o$	1.84848	1.86428			1.89310	1.31	
60 $3s^23p4d\ ^3F_3^o$	1.85133	1.86876			1.89559	1.79	
61 $3s^23p4d\ ^1D_2^o$	1.86138	1.86944		1.88750	1.83331	1.08	
62 $3s^23p4d\ ^3F_4^o$	1.85511	1.87322			1.89891	1.87	
63 $3s^23p4d\ ^3D_1^o$	1.87612	1.88213		1.89120	1.90797	6.22(−1)	
64 $3s^23p4d\ ^3D_2^o$	1.87712	1.88334		1.89260	1.90875	6.43(−1)	
65 $3s3p^2(^4P)3d\ ^5P_3$	1.88460					7.56(−2)	
66 $3s^23p4d\ ^3D_3^o$	1.87893	1.88553		1.89460	1.90992	6.33(−1)	
67 $3s3p^2(^4P)3d\ ^5P_2$	1.88608					7.52(−2)	
68 $3s3p^2(^4P)3d\ ^5P_1$	1.88706					7.49(−2)	
69 $3s^23p4d\ ^3P_2^o$	1.89589	1.89446		1.89660	1.92201	8.19(−1)	
70 $3s^23p4d\ ^3P_1^o$	1.89727	1.89639		1.89710	1.92467	7.68(−1)	
71 $3s^23p4d\ ^3P_0^o$	1.89784	1.89737		1.89740	1.92600	7.33(−1)	
72 $3s^23p5s\ ^3P_0^o$	1.91067	1.91161			1.94313	9.46(−1)	
73 $3s^23p5s\ ^3P_1^o$	1.91230	1.91300			1.94567	8.66(−1)	
74 $3s^23p5s\ ^3P_2^o$	1.91470	1.92003			1.95077	8.21(−1)	
75 $3s^23p4d\ ^1F_3^o$	1.91544	1.92413			1.93565	4.53(−1)	
76 $3s^23p5s\ ^1P_1^o$	1.93395	1.92577			1.91537	4.40(−1)	
77 $3s^23p4d\ ^1P_1^o$	1.94786	1.94594		1.96790	1.97165	4.55(−1)	

Note. Exp.: experimental energy levels. CFF: MCHF calculations of Froese Fischer et al. (2006). TG: CIV3 calculation of Tayal & Gupta (1999). AEM: CIV3 calculation of Abou El-Maaref et al. (2012).

(This table is available in its entirety in machine-readable form.)

Hamiltonian provides the coefficients $C(J\pi;\ \alpha LS\pi)$ that describe the spin–orbit mixing of different LS terms. The term mixing depends both on the spin–orbit interaction and the energy separation between the LS states.

2.2. Collision Calculations

For the scattering calculations, we employed the parallelized version of the BSR code (Zatsarinny 2006). The BSR code uses B-splines as a universal basis to represent the scattering wave functions in the inner region, $r \leqslant a$. Therefore, the R-matrix expansion in this region takes the form

$$\Psi_k(x_1,\ \ldots,\ x_{N+1}) = \mathcal{A}\sum_{ij}\bar{\Phi}_i(x_1,\ \ldots,\ x_N;\ \hat{\boldsymbol{r}}_{N+1}\sigma_{N+1})r_{N+1}^{-1}\,B_j(r_{N+1})a_{ijk} + \sum_i \chi_i(x_1,\ \ldots,\ x_{N+1})b_{ik}. \quad (2)$$

Here, $\mathcal{A}$ denotes the antisymmetrization operator, $\bar{\Phi}_i$ is the channel functions, while the splines, $B_j(r)$, represent the continuum scattering wave functions. The amplitudes of the wave functions at the boundary are given by the coefficient of the last spline. The χ_i function in the above equation are additional $(N+1)$-electron bound states and are included one configuration at a time to ensure completeness of the total trial wave function and to compensate for orthogonality constraints imposed on the continuum orbitals in the R-matrix method. The use of non-orthogonal orbitals allows us to reduce or even to avoid the introduction of additional $(N+1)$-electron terms in the R-matrix expansion. We impose only limited orthogonal conditions to the continuum orbitals. In the present calculations, we only require the orthogonality of continuum orbitals to the bound orbitals in the closed core $1s$, $2s$, and $2p$ shells. We do not impose any orthogonality constraints to the spectroscopic valence orbitals or the correlated orbitals. This procedure eliminates the pseudo-resonance structure from our scattering calculations.

In the present work, the 198 target states in the close-coupling expansions yield a maximum number of 948 different scattering channels in the JK-coupling scheme. The R-matrix boundary radius has been chosen to be $28a_0$, where a_0 is the Bohr radius and the continuum orbitals were represented with the 73 B-splines of the order of 8. All atomic orbitals are very well confined within the chosen R-matrix boundary. The present configuration expansions for the total scattering functions included up to 411,242 individual configuration states. The scattering calculation required the diagonalization of Hamiltonian matrices of sizes up to 69,204. Our numerical calculations included 48 partial waves with total angular momenta up to $2J = 47$. The parallel version of the STGF program (Badnell 2011) has been used for the asymptotic solutions in the outer region to determine the collision strengths. The narrow resonance structures in the energy of excitation thresholds have been resolved using the fine-energy mesh of 0.0001 Ry. The collision strengths do not contain resonances at higher energies where all channels are open. We used a coarse energy grid of 0.2 Ry up to 12.6 Ry in the energy region of all open channels. Altogether, the collision strengths were calculated at 20,510 energies for the colliding electron. The included partial waves were sufficient to achieve convergence for forbidden transitions at all energies. Additional partial wave contributions are needed for the high electron energies in case of the dipole-allowed transitions. These contributions were estimated with a built-in top-up

Table 2
Comparison of Oscillator Strengths and Transition Probabilities (s^{-1}) for Some Dipole Radiative E1 Transitions in S III with Other Calculations

Initial Level	Final Level	g_i	g_f	Present		CFF[a]		Tayal[b]	
				f_L	A_L	f_L	A_L	f_L	A_L
$3s^23p^2\ ^3P$	$-3s3p^3(^2D)\ ^3D^o$	1	3	2.628(−2)	4.125(7)	2.607(−2)	4.023(7)	1.430(−2)	2.243(7)
$3s^23p^2\ ^3P$	$-3s3p^3(^2P)\ ^3P^o$	1	3	4.584(−2)	9.941(7)	4.394(−2)	9.455(7)	3.340(−2)	7.278(7)
$3s^23p^2\ ^3P$	$-3s3p^3(^2P)\ ^1P^o$	1	3	1.135(−2)	4.727(7)	4.323(−4)	1.830(6)	6.840(−3)	2.838(7)
$3s^23p^2\ ^3P$	$-3s3p^3(^4S)\ ^3S^o$	1	3	3.701(−1)	1.569(9)	3.809(−1)	1.657(9)	3.860(−1)	1.639(9)
$3s^23p^2\ ^3P$	$-3s^23p3d\ ^3P^o$	1	3	7.715(−1)	3.514(9)	8.454(−1)	3.851(9)	7.740(−1)	3.465(9)
$3s^23p^2\ ^3P$	$-3s^23p4s\ ^3P^o$	1	3	2.327(−1)	1.114(9)	2.039(−1)	9.829(8)	2.860(−1)	1.378(9)
$3s^23p^2\ ^3P$	$-3s^23p4s\ ^1P^o$	1	3	5.267(−2)	2.579(8)	1.511(−2)	7.392(7)	2.030(−2)	9.944(7)
$3s^23p^2\ ^3P$	$-3s^23p3d\ ^3D^o$	1	3	1.392	6.740(9)	1.425	6.978(9)	1.360	6.665(9)
$3s^23p^2\ ^3P$	$-3s^23p3d\ ^1P^o$	1	3	2.906(−5)	1.741(5)	1.274(−4)	7.899(5)	3.360(−6)	2.025(4)
$3s^23p^2\ ^3P$	$-3s3p^3(^4S)\ ^5S^o$	3	5	3.366(−6)	4.591(3)	3.405(−6)	4.449(3)	3.210(−6)	4.376(3)
$3s^23p^2\ ^3P$	$-3s3p^3(^2D)\ ^3D^o$	3	3	5.840(−3)	2.730(7)	5.785(−3)	2.661(7)	3.100(−3	r.452(7)
$3s^23p^2\ ^3P$	$-3s3p^3(^2D)\ ^3D^o$	3	5	1.960(−2)	5.501(7)	1.947(−2)	5.379(7)	9.980(−3)	2.807(7)
$3s^23p^2\ ^3P$	$-3s3p^3(^2P)\ ^3P^o$	3	5	1.764(−2)	6.843(7)	1.750(−2)	6.736(7)	1.410(−2)	5.498(7)
$3s^23p^2\ ^3P$	$-3s3p^3(^2P)\ ^3P^o$	3	3	1.245(−2)	8.050(7)	1.158(−2)	7.438(7)	9.060(−3)	5.886(7)
$3s^23p^2\ ^3P$	$-3s3p^3(^2P)\ ^3P^o$	3	1	1.538(−2)	2.984(8)	1.515(−2)	2.918(8)	1.080(−2)	2.100(8)
$3s^23p^2\ ^3P$	$-3s^23p3d\ ^1D^o$	3	5	9.805(−5)	4.233(5)	8.837(−5)	3.802(5)	1.970(−4)	8.155(5)
$3s^23p^2\ ^3P$	$-3s^23p3d\ ^3F^o$	3	5	6.387(−5)	3.793(5)	5.574(−5)	3.317(5)	6.690(−5)	3.978(5)
$3s^23p^2\ ^3P$	$-3s3p^3(^2P)\ ^1P^o$	3	3	1.370(−2)	1.704(8)	5.256(−5)	6.650(5)	1.100(−2)	1.375(8)
$3s^23p^2\ ^3P$	$-3s3p^3(^4S)\ ^3S^o$	3	3	3.497(−1)	4.428(9)	3.586(−1)	4.665(9)	3.600(−1)	4.572(9)
$3s^23p^2\ ^3P$	$-3s^23p3d\ ^3P^o$	3	1	2.374(−1)	9.686(9)	2.502(−1)	1.020(10)	2.520)-1)	1.008(10)
$3s^23p^2\ ^3P$	$-3s^23p3d\ ^3P^o$	3	3	1.539(−1)	2.094(9)	1.744(−1)	2.374(9)	1.570(−1)	2.095(9)
$3s^23p^2\ ^3P$	$-3s^23p3d\ ^3P^o$	3	5	3.844(−1)	3.138(9)	4.007(−1)	3.279(9)	3.540(−1)	2.859(9)
$3s^23p^2\ ^3P$	$-3s^23p4s\ ^3P^o$	3	3	3.004(−3)	4.297(7)	1.552(−3)	2.237(7)	2.490(−4)	3.589(6)
$3s^23p^2\ ^3P$	$-3s^23p4s\ ^3P^o$	3	1	4.454(−2)	1.910(9)	3.176(−2)	1.373(9)	2.810(−2)	1.214(9)
$3s^23p^2\ ^3P$	$-3s^23p4s\ ^3P^o$	3	5	1.525(−1)	1.316(9)	1.144(−1)	9.928(8)	8.960(−1)	7.784(9)
$3s^23p^2\ ^3P$	$-3s^23p4s\ ^1P^o$	3	3	1.675(−5)	2.451(5)	9.482(−4)	1.387(7)	7.810(−4)	1.142(7)
$3s^23p^2\ ^3P$	$-3s^23p3d\ ^3D^o$	3	3	4.494(−1)	6.500(9)	4.470(−1)	6.541(9)	4.470(−1)	6.523(9)
$3s^23p^2\ ^3P$	$-3s^23p3d\ ^3D^o$	3	5	1.041	9.047(9)	1.069	9.397(9)	3.260(−1)	2.850(9)
$3s^23p^2\ ^3P$	$-3s3p^3(^2D)\ ^1D^o$	3	5	6.531(−4)	6.013(6)	6.492(−4)	6.101(6)	8.140(−4)	7.608(6)
$3s^23p^2\ ^3P$	$-3s^23p3d\ ^1P^o$	3	3	1.560(−5)	2.794(5)	9.148(−5)	1.696(6)	1.890(−5)	3.416(5)
$3s^23p^2\ ^3P$	$-3s3p^3(^4S)\ ^5S^o$	5	5	5.730(−6)	1.279(4)	5.750(−6)	1.231(4)	5.470(−6)	1.222(4)
$3s^23p^2\ ^3P$	$-3s3p^3(^2D)\ ^3D^o$	5	3	1.866(−4)	1.436(6)	1.814(−4)	1.375(6)	9.580(−5)	7.375(5)
$3s^23p^2\ ^3P$	$-3s3p^3(^2D)\ ^3D^o$	5	5	3.095(−3)	1.430(7)	3.050(−3)	1.388(7)	1.470(−3)	6.823(6)
$3s^23p^2\ ^3P$	$-3s3p^3(^2D)\ ^3D^o$	5	7	2.061(−2)	6.808(7)	2.047(−2)	6.663(7)	1.100(−2)	3.642(7)
$3s^23p^2\ ^3P$	$-3s3p^3(^2P)\ ^3P^o$	5	5	3.406(−2)	2.178(8)	3.368(−2)	2.140(8)	2.710(−2)	1.738(8)
$3s^23p^2\ ^3P$	$-3s3p^3(^2P)\ ^3P^o$	5	3	1.077(−2)	1.148(8)	1.126(−2)	1.193(8)	7.650(−3)	8.189(7)
$3s^23p^2\ ^3P$	$-3s^23p3d\ ^1D^o$	5	5	2.195(−5)	1.563(5)	1.827(−5)	1.298(5)	4.520(−5)	3.082(5)
$3s^23p^2\ ^3P$	$-3s^23p3d\ ^3F^o$	5	5	1.356(−5)	1.330(5)	1.185(−5)	1.166(5)	1.470(−5)	1.449(5)
$3s^23p^2\ ^3P$	$-3s^23p3d\ ^3F^o$	5	7	1.080(−4)	7.608(5)	9.402(−5)	6.638(5)	1.100(−4)	7.819(5)
$3s^23p^2\ ^3P$	$-3s3p^3(^2P)\ ^1P^o$	5	3	2.154(−2)	4.429(8)	7.940(−4)	1.662(7)	1.790(−2)	3.667(8)
$3s^23p^2\ ^3P$	$-3s3p^3(^4S)\ ^3S^o$	5	3	3.140(−1)	6.574(9)	3.201(−1)	6.891(9)	3.220(−1)	6.763(9)
$3s^23p^2\ ^3P$	$-3s^23p3d\ ^3P^o$	5	3	1.932(−1)	4.348(9)	1.884(−1)	4.247(9)	1.980(−1)	4.386(9)
$3s^23p^2\ ^3P$	$-3s^23p3d\ ^3P^o$	5	5	5.504(−1)	7.433(9)	5.699(−1)	7.720(9)	5.130(−1)	6.862(9)
$3s^23p^2\ ^3P$	$-3s^23p4s\ ^3P^o$	5	3	1.752(−2)	4.147(8)	1.221(−2)	2.914(8)	1.490(−2)	3.563(8)
$3s^23p^2\ ^3P$	$-3s^23p4s\ ^3P^o$	5	5	9.954(−3)	1.421(8)	2.778(−3)	3.993(7)	3.760(−2)	5.398(8)
$3s^23p^2\ ^3P$	$-3s^23p4s\ ^1P^o$	5	3	3.580(−3)	8.667(7)	2.434(−4)	5.897(6)	4.330(−4)	1.049(7)
$3s^23p^2\ ^3P$	$-3s^23p3d\ ^3D^o$	5	3	2.802(−2)	6.705(8)	2.647(−2)	6.413(8)	2.860(−2)	6.910(8)
$3s^23p^2\ ^3P$	$-3s^23p3d\ ^3D^o$	5	5	3.183(−1)	4.578(9)	3.097(−1)	4.510(9)	3.230(−1)	4.670(9)
$3s^23p^2\ ^3P$	$-3s^23p3d\ ^3D^o$	5	7	1.372	1.411(10)	1.380	1.437(10)	1.380	1.426(10)
$3s^23p^2\ ^3P$	$-3s3p^3(^2D)\ ^1D^o$	5	5	2.136(−4)	3.254(6)	2.689(−4)	4.186(6)	1.930(−4)	2.988(6)
$3s^23p^2\ ^3P$	$-3s^23p3d\ ^1F^o$	5	7	1.430(−4)	1.675(6)	1.633(−4)	1.935(6)	1.960(−4)	2.308)6)
$3s^23p^2\ ^1D$	$-3s3p^3(^2D)\ ^3D^o$	5	3	7.760(−6)	4.559(4)	7.960(−6)	4.566(4)	9.950(−6)	5.861(4)
$3s^23p^2\ ^1D$	$-3s3p^3(^2D)\ ^3D^o$	5	5	1.215(−6)	4.288(3)	1.657(−6)	5.706(3)	8.100(−7)	2.870(3)
$3s^23p^2\ ^1D$	$-3s3p^3(^2D)\ ^3D^o$	5	7	2.089(−5)	5.272(4)	2.129(−5)	5.243(4)	1.590(−5)	4.029(4)
$3s^23p^2\ ^1D$	$-3s3p^3(^2P)\ ^3P^o$	5	5	2.171(−5)	1.107(5)	1.956(−5)	9.846(4)	5.580(−4)	2.857(6)
$3s^23p^2\ ^1D$	$-3s3p^3(^2P)\ ^3P^o$	5	3	9.733(−6)	8.274(4)	1.105(−5)	9.271(4)	9.260(−6)	7.917(4)
$3s^23p^2\ ^1D$	$-3s^23p3d\ ^1D^o$	5	5	2.378(−2)	1.367(8)	2.377(−2)	1.355(8)	7.590(−2)	4.159(8)
$3s^23p^2\ ^1D$	$-3s^23p3d\ ^3F^o$	5	5	4.356(−5)	3.567(5)	3.970(−5)	3.247(5)	6.320(−5)	5.193(5)

Table 2
(Continued)

Initial Level	Final Level	g_i	g_f	Present		CFF[a]		Tayal[b]	
				f_L	A_L	f_L	A_L	f_L	A_L
$3s^23p^2\ ^1D$	$-3s^23p3d\ ^3F^o$	5	7	7.533(−5)	4.429(5)	5.964(−5)	3.500(5)	7.440(−5)	4.380(5)
$3s^23p^2\ ^1D$	$-3s3p^3(^2P)\ ^1P^o$	5	3	3.219(−1)	5.639(9)	3.414(−1)	6.073(9)	2.800(−1)	4.883(9)
$3s^23p^2\ ^1D$	$-3s3p^3(^4S)\ ^3S^o$	5	3	1.879(−2)	3.355(8)	1.441(−2)	2.641(8)	1.320(−2)	2.358(8)
$3s^23p^2\ ^1D$	$-3s^23p3d\ ^3P^o$	5	3	3.522(−5)	6.802(5)	9.868(−5)	1.901(6)	1.710(−4)	3.241(6)
$3s^23p^2\ ^1D$	$-3s^23p3d\ ^3P^o$	5	5	1.413(−5)	1.637(5)	1.171(−5)	1.356(5)	4.220(−5)	4.844(5)
$3s^23p^2\ ^1D$	$-3s^23p4s\ ^3P^o$	5	3	3.429(−2)	6.991(8)	1.057(−2)	2.166(8)	1.150(−2)	2.356(8)
$3s^23p^2\ ^1D$	$-3s^23p4s\ ^3P^o$	5	5	6.457(−4)	7.945(6)	5.615(−4)	6.934(6)	1.300(−3)	1.617(7)
$3s^23p^2\ ^1D$	$-3s^23p4s\ ^1P^o$	5	3	9.329(−2)	1.949(9)	1.191(−1)	2.481(9)	1.420(−1)	2.960(9)
$3s^23p^2\ ^1D$	$-3s^23p3d\ ^3D^o$	5	3	4.524(−6)	9.334(4)	7.050(−5)	1.468(6)	1.200(−4)	2.497(6)
$3s^23p^2\ ^1D$	$-3s^23p3d\ ^3D^o$	5	5	3.685(−4)	4.570(6)	3.947(−4)	4.942(6)	2.640(−7)	3.298(3)
$3s^23p^2\ ^1D$	$-3s^23p3d\ ^3D^o$	5	7	1.557(−4)	1.380(6)	1.794(−4)	1.605(6)	2.210(−4)	1.978(6)
$3s^23p^2\ ^1D$	$-3s3p^3(^2D)\ ^1D^o$	5	5	9.945(−1)	1.312(10)	1.001	1.347(10)	9.490(−1)	1.274(10)
$3s^23p^2\ ^1D$	$-3s^23p3d\ ^1F^o$	5	7	1.334	1.360(10)	1.353	1.392(10)	1.330	1.359(10)
$3s^23p^2\ ^1D$	$-3s^23p3d\ ^1P^o$	5	3	1.836(−2)	4.768(8)	1.746(−2)	4.695(8)	4.140(−2)	1.084(9)
$3s^23p^2\ ^1S$	$-3s3p^3(^2D)\ ^3D^o$	1	3	1.432(−6)	1.029(3)	1.326(−6)	9.195(2)	9.380(−7)	6.738(2)
$3s^23p^2\ ^1S$	$-3s3p^3(^2P)\ ^3P^o$	1	3	2.324(−5)	2.650(4)	2.217(−5)	2.477(4)	2.210(−5)	2.537(4)
$3s^23p^2\ ^1S$	$-3s3p^3(^2P)\ ^1P^o$	1	3	6.942(−4)	1.857(6)	6.448(−4)	1.751(6)	2.120(−2)	5.653(7)
$3s^23p^2\ ^1S$	$-3s3p^3(^4S)\ ^3S^o$	1	3	4.584(−5)	1.254(5)	5.254(−5)	1.476(5)	7.860(−4)	2.154(6)
$3s^23p^2\ ^1S$	$-3s^23p3d\ ^3P^o$	1	3	1.469(−5)	4.392(4)	6.006(−7)	1.786(3)	6.190(−5)	1.810(5)
$3s^23p^2\ ^1S$	$-3s^23p4s\ ^3P^o$	1	3	1.532(−2)	4.872(7)	4.376(−3)	1.396(7)	1.880(−3)	6.016(6)
$3s^23p^2\ ^1S$	$-3s^23p4s\ ^1P^o$	1	3	4.443(−2)	1.452(8)	5.266(−2)	1.710(8)	2.320(−2)	7.569(7)
$3s^23p^2\ ^1S$	$-3s^23p3d\ ^3D^o$	1	3	2.270(−7)	7.315(2)	5.799(−5)	1.884(5)	1.340(−6)	4.373(3)
$3s^23p^2\ ^1S$	$-3s^23p3d\ ^1P^o$	1	3	2.643	1.103(10)	2.722	1.178(10)	2.710	1.138(10)

Notes.
[a] MCHF calculations of Froese Fischer et al. (2006).
[b] CIV3 calculation of Tayal (1997b).

procedures in the STGF code based on the Coulomb-Bethe method and/or on geometric series approximation. For even higher energies, we extrapolated collision strengths Ω using the well-known asymptotic energy dependence of the various types of transitions (Tayal & Zatsarinny 2011, 2014).

To obtain effective collision strengths $\Upsilon(T_e)$, we convoluted the collision strength, Ω, with a Maxwellian distribution for an electron temperature, T_e, i.e.,

$$\Upsilon_{i-j}(T_e) = \int_{E_{th}}^{\infty} dE\ \Omega_{i-j}(E)\exp\left(\frac{E - E_{th}}{kT_e}\right). \quad (3)$$

Here, E_{th} is the $i - j$ transition energy and k is the Boltzmann constant. We calculated Υ for temperatures from 10^3 to 10^6 K that are suitable for astrophysical and other plasma applications. It should be noted that Grieve et al. (2014) studied the presence of κ-distribution of electron energies for the Io plasma torus but did not find any definite evidence for the deviation from the Maxwellian distribution. They adopted the method of Nicholls et al. (2013) in their calculations of averaged collision strengths over several κ electron energy distributions.

3. Results and Discussion

3.1. Radiative Transition Rates

We provide target level excitation energies for the 198 S III levels from the present calculation together with the available experimental values of Johansson et al. (1992) and from the National Institute of Standards and Technology compilation[4] in Table 1. The order of the $3s^23p4s\ ^1P_1^o$ level from our calculation does not agree with the experiment, perhaps due to the proximity of the levels resulting in strong mixing. We index the energy levels in the order of experimental energies where available in Table 1 because we used experimental energies in our scattering calculations and refer to these indices to tabulate effective collision strengths. There are many energy levels included in our calculation for which no experimental values are available. Many of these levels were also not considered by Grieve et al. (2014). For example, the odd parity levels of the $3s^23p4d$ configuration are indexed 42–53 in their Table 2, while these levels have indices 60–65 and 69–77 in the present Table 1. We also compare the present calculated energy levels with other available calculations of Froese Fischer et al. (2006; CFF), Tayal & Gupta (1999; TG), and Abou El-Maaref et al. (2012; AEM). Froese Fischer et al. (2006) and the present calculations were performed in the Breit–Pauli approach using the MCHF code (Froese Fischer 2007) and the MCHF plus CI computer code with non-orthogonal orbitals. The Breit–Pauli CIV3 computer code (Hibbert 1975; Glass & Hibbert 1978) was used by Tayal & Gupta (1999) and Abou El-Maaref et al. (2012) in their calculations of energy levels and radiative rates. Our calculated target energies differ from the experimental values from 0.003 to 0.027 Ry. The largest difference of 0.0268 Ry is for the $3s^23p3d\ ^1P_1^o$ level and is caused by the

[4] http://physics.nist.gov/asd3

Table 3
Oscillator Strengths (f_L, f_V) and Radiative Rates (A_L in s^{-1}) for Electric Dipole (E1) Transitions among LSJ Levels in S III

Initial Level	Final Level	g_i	g_f	f_L	f_V	A_L
$3s^23p^2\ ^3P$	$-3s3p^3(^2D)\ ^3D^o$	1	3	2.628E−02	2.411E−02	4.125E+07
$3s^23p^2\ ^3P$	$-3s3p^3(^2P)\ ^3P^o$	1	3	4.584E−02	4.472E−02	9.941E+07
$3s^23p^2\ ^3P$	$-3s3p^3(^2P)\ ^1P^o$	1	3	1.135E−02	1.135E−02	4.727E+07
$3s^23p^2\ ^3P$	$-3s3p^3(^4S)\ ^3S^o$	1	3	3.701E−01	3.736E−01	1.569E+09
$3s^23p^2\ ^3P$	$-3s^23p3d\ ^3P^o$	1	3	7.715E−01	7.724E−01	3.514E+09
$3s^23p^2\ ^3P$	$-3s^23p4s\ ^3P^o$	1	3	2.327E−01	2.328E−01	1.114E+09
$3s^23p^2\ ^3P$	$-3s^23p4s\ ^1P^o$	1	3	5.267E−02	5.224E−02	2.579E+08
$3s^23p^2\ ^3P$	$-3s^23p3d\ ^3D^o$	1	3	1.392E+00	1.411E+00	6.740E+09
$3s^23p^2\ ^3P$	$-3s^23p3d\ ^1P^o$	1	3	2.906E−05	1.682E−05	1.741E+05
$3s^23p^2\ ^3P$	$-3s^23p4d\ ^3D^o$	1	3	7.673E−02	7.840E−02	7.303E+08
$3s^23p^2\ ^3P$	$-3s^23p4d\ ^3P^o$	1	3	1.318E−02	1.338E−02	1.269E+08
$3s^23p^2\ ^3P$	$-3s^23p5s\ ^3P^o$	1	3	1.743E−02	1.683E−02	1.708E+08
$3s^23p^2\ ^3P$	$-3s^23p5s\ ^1P^o$	1	3	2.439E−03	2.358E−03	2.422E+07

(This table is available in its entirety in machine-readable form.)

slower convergence of the CI expansion. Our energy levels are in very good agreement with the calculation of Froese Fischer et al. (2006), which in turn shows similar variations with the experimental values. It may be noted that Froese Fischer et al. (2006) results are available only for the first 40 levels. The present MCHF plus CI non-orthogonal results and the MCHF calculation of Froese Fischer et al. (2006) are generally in better agreement with the experiment than the CIV3 calculations of Tayal & Gupta (1999) and Abou El-Maaref et al. (2012). In Table 1, we also show lifetimes of all excited levels and compare our lifetimes with available values of Froese Fischer et al. (2006). There is an excellent agreement for most excited levels between the two calculations except for the energy levels of the $3s^23p4s\ ^3P^o$ term.

In Table 2, we compare present oscillator strengths and transition probabilities in length formulation for some dipole-allowed E1 transitions with the calculations of Froese Fischer et al. (2006) and Tayal (1997b). We displayed results for the transitions from the $3s^23p^2\ ^3P_{0,1,2}$, $^1D_2$, and $^1S_0$ levels to all the levels of the $3s3p^3\ ^5S^o$, $^3D^o$, $^3P^o$, $^3S^o$, $^1D^o$, $^1P^o$, $3s^23p3d\ ^3F^o$, $^3D^o$, $^3P^o$, $1F^o$, $^1D^o$, $^1P^o$, $3s^23p4s\ ^3P^o$, and $^1P^o$ terms. The agreement with other calculations is very good for strong transitions. The oscillator strengths for transitions with values larger than 0.1 agree within 20% for most transitions. However, only approximately half of the transitions with oscillator strengths less than 0.1 from various theories agree within 20%. The oscillator strengths for spin-changing transitions are especially influenced by various types of correlation effects and interactions. The mixing due to the spin–orbit interaction drives intercombination transitions. There are large deviations between the three calculations for weaker transitions where configurations with smaller mixing coefficients in CI expansions normally play an important role due to cancellation effects in larger mixing coefficients. As a result, the radiative rates for weaker transitions are less reliable. We listed the present oscillator strengths in both length and velocity formulations and transition probabilities in length formulation for all transitions between energy levels of up to the $3s3p^2(^4P)4s\ ^3P$ term in Table 3. The agreement between the length and velocity forms of oscillator strengths is normally considered to be an indicator of the quality of wave functions. The present length and velocity forms agree to within 20% for most E1 transitions with oscillator strength values $\geqslant$0.01. Approximately 20% of transitions with values of oscillator strengths between 0.1 and 0.01 show deviations larger than 20%. Almost half of the transitions with oscillator strengths smaller than 0.01 show an agreement of 20% or better between lengths and velocity values, while the other weaker transitions display larger dispersion. The entire contents of Table 3 are given in machine-readable format and are fully explained in the associated ReadMe file.

The theoretical calculations of length oscillator strengths and transition probabilities for forbidden E2 and M1 transitions among ground configuration $3s^23p^2$ levels are reported in Table 4. The present MCHF results are compared with the MCHF calculation of Froese Fischer et al. (2006). The transition probabilities for M1 and E2 transitions are very sensitive to transition energies and scale as ΔE^3 and ΔE^5, respectively. Thus, small differences in transition energies can quickly result in large differences in transition probabilities. In Table 3 we present length values because the length and velocity forms for forbidden transitions may differ substantially and therefore does not provide much additional indication about the accuracy of the results. The overall agreement with the calculation of Froese Fischer et al. (2006) is satisfactory for several E2 and M1 transitions. The transition probabilities for E2 $3s^23p^2\ ^1D_2$–$3s^23p^2\ ^1S_0$ transition and M1 forbidden transitions $3s^23p^2\ ^3P_1$–$3s^23p^2\ ^1S_0$, $3s^23p^2\ ^3P_2$–$3s^23p^2\ ^1D_2$, and $3s^23p^2\ ^3P_1$–$3s^23p^2\ ^1D_2$ have significant strengths. The agreement with the calculation of Froese Fischer et al. (2006) is well within 10% for these and some other transitions. The comparison between the two calculations can provide an accuracy estimate of transition probabilities of forbidden transitions to some extent.

3.2. Electron Collision Rates

Our scattering model contains 198 fine-structure levels of S III and is referred as BSR-198 in the following discussion of collision rates. The 53 fine-structure levels (29 LS states) intermediate coupling calculations of Hudson et al. (2012) and Grieve et al. (2014) will be denoted by RM-53. The LS-coupled plus algebraic transformation to intermediate coupling calculations of Tayal & Gupta (1999) and Galaýs et al. (1995)

Table 4
Comparison of Oscillator Strengths and Transition Probabilities (s^{-1}) for Forbidden M1 and E2 Transitions among the Fine-structure Levels of the Ground $3s^23p^2$ Configuration in S III with Those Calculated by Froese Fischer et al. (2006)

Initial Level	Final Level	Type	Present		CFF[a]	
			A_L	f_L	A_L	f_L
$3s^23p^2\ ^3P_0$	$3s^23p^2\ ^3P_1$	$M1$	3.09(−04)	2.09(−08)	3.42(−04)	2.1(−08)
$3s^23p^2\ ^3P_0$	$3s^23p^2\ ^3P_2$	$E2$	2.11(−08)	2.96(−13)	2.28(−08)	3.11(−13)
$3s^23p^2\ ^3P_0$	$3s^23p^2\ ^1D_2$	$E2$	8.97(−06)	4.69(−13)	5.64(−06)	3.20(−13)
$3s^23p^2\ ^3P_1$	$3s^23p^2\ ^3P_2$	$E2$	5.34(−09)	5.99(−14)	5.47(−09)	6.10(−14)
$3s^23p^2\ ^3P_1$	$3s^23p^2\ ^3P_2$	$M1$	1.42(−03)	1.60(−08)	1.43(−03)	1.59(−08)
$3s^23p^2\ ^3P_1$	$3s^23p^2\ ^1D_2$	$E2$	4.25(−05)	7.74(−13)	4.30(−05)	8.53(−13)
$3s^23p^2\ ^3P_1$	$3s^23p^2\ ^1D_2$	$M1$	2.00(−02)	3.65(−10)	1.95(−02)	3.87(−10)
$3s^23p^2\ ^3P_1$	$3s^23p^2\ ^1S_0$	$M1$	6.81(−01)	4.40(−10)	6.88(−01)	4.64(−10)
$3s^23p^2\ ^3P_2$	$3s^23p^2\ ^1D_2$	$E2$	2.76(−04)	3.27(−12)	2.35(−04)	3.05(−12)
$3s^23p^2\ ^3P_2$	$3s^23p^2\ ^1D_2$	$M1$	5.30(−02)	6.29(−10)	5.13(−02)	6.67(−10)
$3s^23p^2\ ^3P_2$	$3s^23p^2\ ^1S_0$	$E2$	9.60(−03)	3.85(−12)	9.53(−03)	4.00(−12)
$3s^23p^2\ ^1D_2$	$3s^23p^2\ ^1S_0$	$E2$	2.30(+00)	2.66(−09)	2.19(+00)	2.57(−09)

Note.
[a] MCHF calculations of Froese Fischer et al. (2006).

considered 49 fine-structure levels (27 LS states) and 17 LS target states, respectively. These will be denoted by RM-49 and RM-17. The collision calculations of Tayal & Gupta (1999) did not include four fine-structure levels of $3s^23p4d\ ^3F^o_{2,3,4}$ and $^1F^o_3$ because of computer resource limitations at that time. These levels were later included by Hudson et al. (2012) and Grieve et al. (2014) and were found to impact the collision strengths for transitions to higher excitation levels of $3s^23p4d\ ^3P^o_{0,1,2}$ of astrophysical importance. They noted that the resonances converging to the $3s^23p4d\ ^3F^o_{2,3,4}$ and $^1F^o_3$ are responsible for the significant discrepancies with the results of Tayal & Gupta (1999). However, Hudson et al. (2012) and Grieve et al. (2014) also did not consider all $n = 4$ levels and the other intervening $3s^23p5s\ ^3P^o_{0,1,2}$ and $^1P^o_1$ levels of odd parity. They also omitted other even parity levels of the $3s3p^2(^4P)3d$, $3s3p^2(^2D)3d$, and $3p^4$ configurations that lie below the highest excitation level of $3s^23p4d\ ^1P^o_1$ of their calculation. It is worthwhile to check the effects of coupling with these intervening levels below the $3s^23p4d\ ^1P^o_1$ level and many more levels above the $3s^23p4d\ ^1P^o_1$ level with the $n = 5$, $l = 0$–2 and $n = 6$, $l = 0$, as well as some other levels belonging to the $3s3p^2nl$ $n = 3$–5 and $3p^4$ configurations. We employed flexible term-dependent non-orthogonal orbitals to obtain accurate target descriptions and included fine-structure effects in the close-coupling expansions. Our calculated target excitation energies are in very good agreement with measured values. We adjusted theoretical thresholds to experimental values where available to further improve positions of resonance structures in the present scattering calculations. We used a fine-energy grid of 0.0001 Ry to delineate resonances in the calculation of collision strengths that are generally more important for the forbidden and intercombination transitions than the dipole-allowed transitions.

The collision strength for the forbidden $3s^23p^2\ ^3P_0$–$3s^23p^2\ ^3P_1$ (1–2) fine-structure transition has been presented in the resonant energy region below the highest excitation threshold in Figure 1. The collision strength shows strong resonance structures in the energy region below the $3s^23p3d\ ^1P^o_1$ threshold around 1.496 Ry. However, resonances are very weak in the

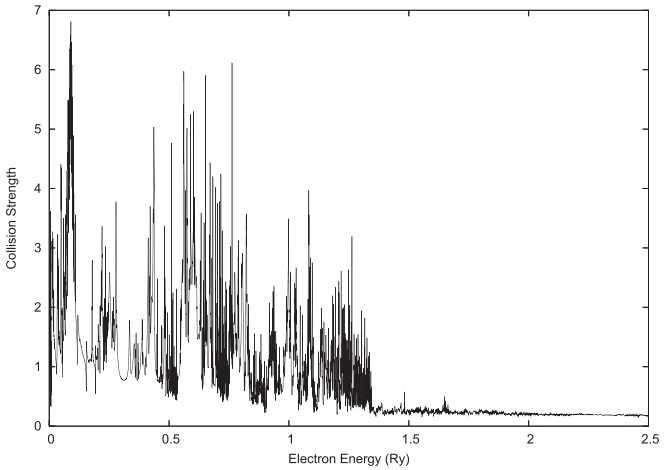

Figure 1. Collision strength for the forbidden fine-structure $3s^23p^2\ ^3P_0$–$^3P_1$ transition in S III as a function of electron energy (in Ry). The fine-energy mesh is used to resolve resonances at low energies.

energy region of higher excitation thresholds. The visual comparison with the collision strengths of Hudson et al. (2012) given in their Figure 1 shows good agreement for the positions and magnitudes of all major resonances. The present collision strengths show somewhat denser resonance structures than the calculation of Hudson et al. (2012) because of the resolution of narrower resonances. The collision strength displays smooth variation with incident electron energy in the region of all open channels. The effective collision strengths for the forbidden $3s^23p^2\ ^3P_0$–$3s^23p^2\ ^3P_1$ (1–2) and $3s^23p^2\ ^3P_1$–$3s^23p^2\ ^3P_2$ (2-3) transitions have been compared with other available calculations of Hudson et al. (2012), Tayal & Gupta (1999), and Galaýs et al. (1995) as a function of the electron temperature from log $T = 3.0$ to 6.0 in Figure 2. The present BSR-198 results are displayed by a solid curve, and the calculations of Hudson et al. (2012), Tayal & Gupta (1999), and Galaýs et al. (1995) are represented by long-dashed, short-dashed, and dotted curves, respectively. The RM-49 calculation of Tayal & Gupta (1999) shows substantial differences with other three

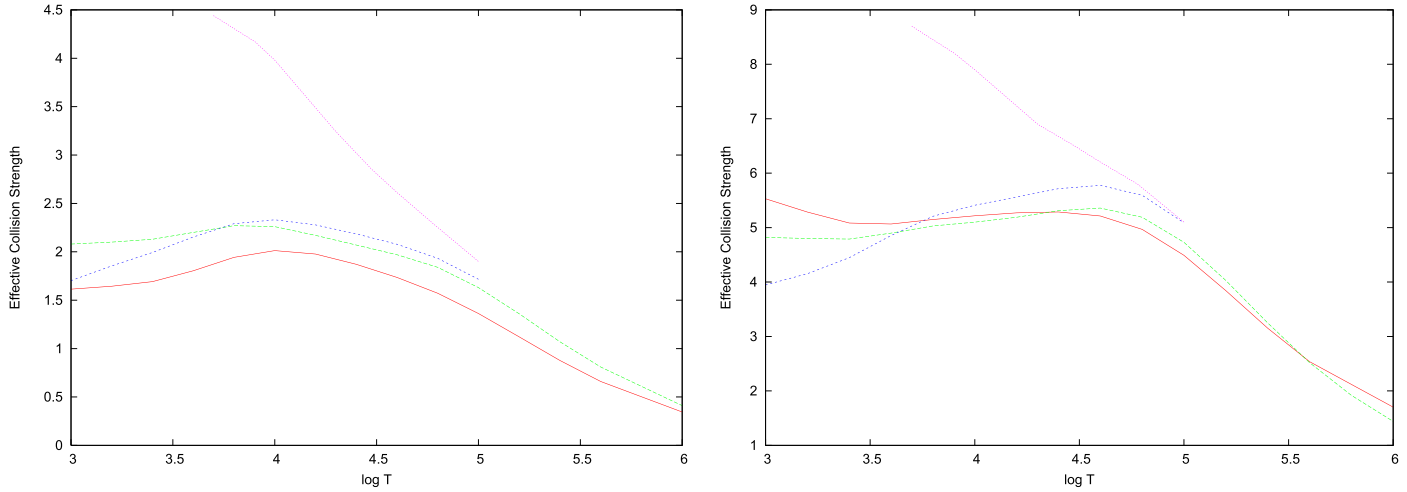

Figure 2. Effective collision strength for the forbidden fine-structure (a) $3s^23p^2\ ^3P_0$–$3s^23p^2\ ^3P_1$ (1–2) and (b) $3s^23p^2\ ^3P_1$–$3s^23p^2\ ^3P_2$ (2–3) transitions in S III as a function of the electron temperature. Solid curve: present BSR-198 model; long-dashed curve: RM-53 model; short-dashed curve: RM-48 model; dotted curve: RM-17 model.

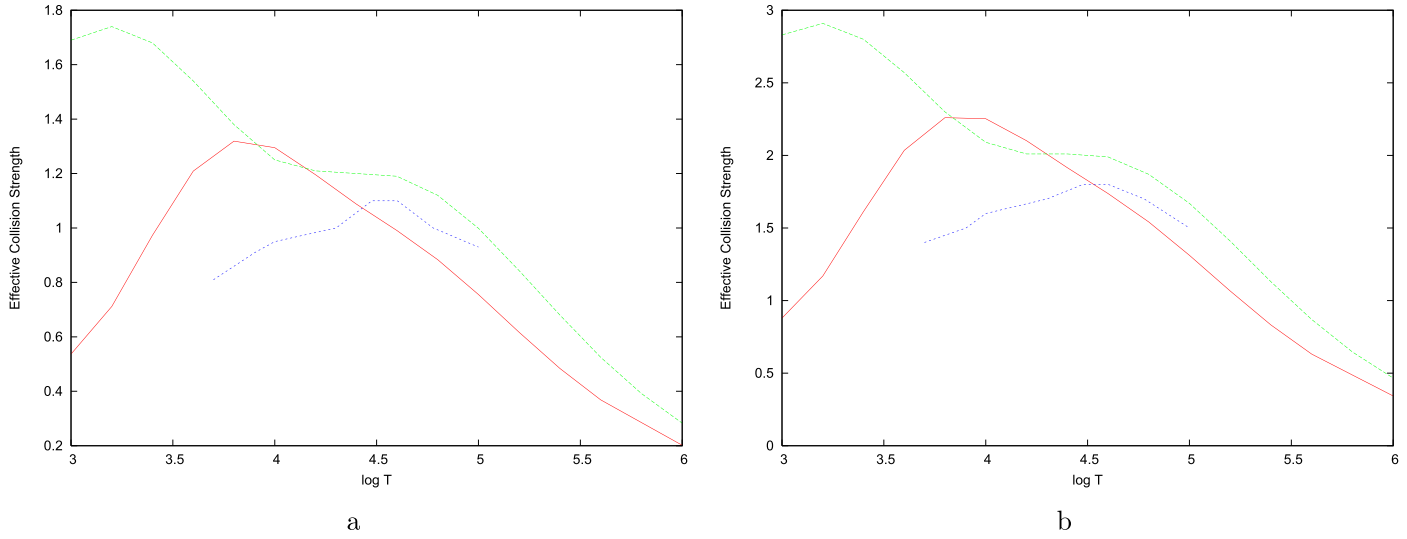

Figure 3. Effective collision strength for the spin-forbidden fine-structure (a) $3s^23p^2\ ^3P_1$–$3s3p^3\ ^5S^o_2$ (2–6) and (b) $3s^23p^2\ ^3P_2$–$3s3p^3\ ^5S^o_2$ (3–6) transitions in S III as a function of the electron temperature. Solid curve: present BSR-198 model; long-dashed curve: RM-53 model; short-dashed curve: RM-48 model.

calculations in the low temperature region, primarily because of the omission of collision strengths in the low energy region below 0.1 Ry, as noted by Hudson et al. (2012). The larger discrepancies between the present BSR-198 results and the RM-53 calculation of Hudson et al. (2012) at log $T = 3.0$ may be due to a slight shift in resonance structures. As the temperature increases, two calculations begin to converge to each other, and the difference becomes smaller.

The effective collision strengths for spin-forbidden (a) $3s^23p^2\ ^3P_1$–$3s3p^3\ ^5S^o_2$ (2–6) and (b) $3s^23p^2\ ^3P_2$–$3s3p^3\ ^5S^o_2$ (3–6) transitions are shown in Figure 3. The resonance structures contribute substantially to the collision strengths of the spin-forbidden transitions. Our results differ from the calculation of Grieve et al. (2014) by up to 65% at lower temperatures and agree very well at middle temperatures around log $T = 4.0$. Figure 4 displays the results of BSR-198, RM-53, and RM-48 for the dipole-allowed (a) $3s^23p^2\ ^3P_2$–$3s3p^3\ ^3P^o_2$ (3–10) and (b) $3s^23p^2\ ^3P_2$–$3s3p^3\ ^3P^o_1$ (3–11) transitions. The collision strengths for the dipole-allowed transitions are directly proportional to the oscillator strengths at high electron energies. The peak of effective collision strength from the BSR-198 is shifted to a lower temperature than the calculations of Grieve et al. (2014) and Tayal & Gupta (1999). It is perhaps caused by the better description of target energies and adjustments of thresholds to measured energies. The three calculations show overall good agreement and agree to about 20%. Finally, we compare the present effective collision strength with the work of Tayal & Gupta (1999) and Grieve et al. (2014) in Figure 5 for the dipole-allowed (a) $3s^23p^2\ ^3P_2$–$3s^23p4d\ ^3P^o_2$ (3–69) and (b) $3s^23p^2\ ^3P_2$–$3s^23p4d\ ^3P^o_1$ (3–70) transitions. The results from the present and Grieve et al. (2014) calculations exhibit large discrepancies with the

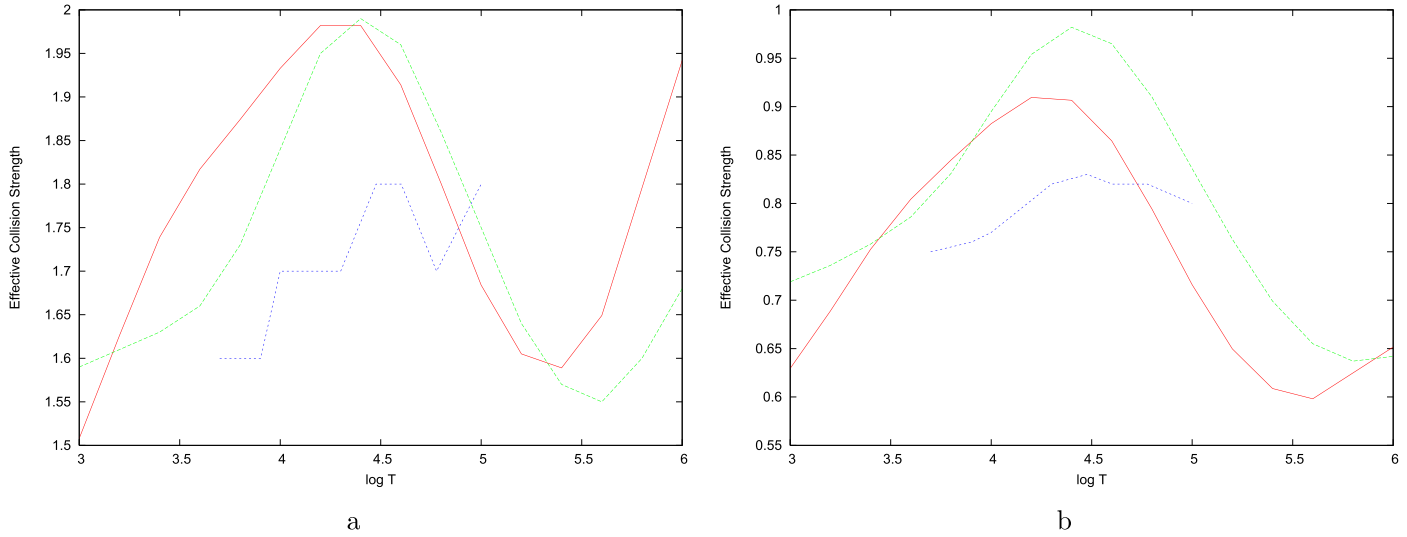

Figure 4. Effective collision strength for the dipole-allowed fine-structure (a) $3s^2 3p^2\ ^3P_2$–$3s3p^3\ ^3P_2^o$ (3–10) and (b) $3s^2 3p^2\ ^3P_2$–$3s3p^3\ ^3P_1^o$ (3–11) transitions in S III as a function of the electron temperature. Solid curve: present BSR-198 model; long-dashed curve: RM-53 model; short-dashed curve: RM-48 model.

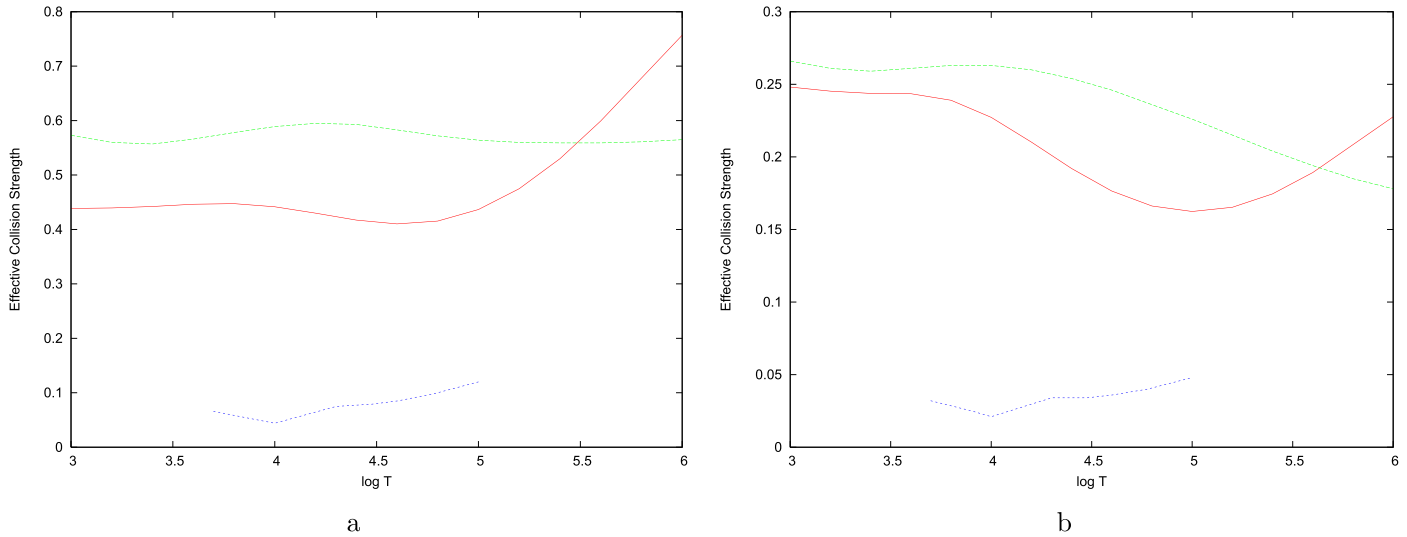

Figure 5. Effective collision strength for the dipole-allowed fine-structure (a) $3s^2 3p^2\ ^3P_2$–$3s^2 3p4d\ ^3P_2^o$ (3–69) and (b) $3s^2 3p^2\ ^3P_2$–$3s^2 3p4d\ ^3P_2^o$ (3–70) transitions. Solid curve, present BSR-198 model; long-dashed curve, RM-53 model; short-dashed curve, RM-48 model.

calculation of Tayal & Gupta (1999) as they omitted important resonances converging to the $3s^2 3p4d\ ^3F^o$ levels. Our results show some differences in the shape and magnitude with the calculation of Grieve et al. (2014). For example, our results show an increasing trend at higher temperatures, as expected of a dipole-allowed transition, while the results of Grieve et al. (2014) decrease with the temperature at higher temperatures, especially for the dipole-allowed $3s^2 3p^2\ ^3P_2$–$3s^2 3p4d\ ^3P_1^o$ (3–70) transition.

We compare present BSR-198 results with the effective collision strengths from the previous RM-53 calculation of Grieve et al. (2014) at three different 10^3, 10^4, and 10^5 K temperatures for all available transitions between 53 fine-structure levels in Figure 6. It is clear from the figure that the average deviations are 22.7%, 20.9%, and 23.2% at three temperatures. Thus, the agreement between the two calculations becomes worse at lower and higher temperatures. At low temperatures, the effective collision strengths depend on the near-threshold resonance structures in the low energy region. The near-threshold resonance structure is impacted by the target excitation energies and the size of computer code (CC) expansions. We used the experimental excitation thresholds where available and employed an extensive CC expansion. The narrower resonances are not expected to contribute significantly to the effective collision strengths determined by convoluting the collision strengths. The resonance contribution diminishes at higher electron energies. As seen from Figure 6, agreement improves for the intermediate temperatures around $T = 10^4$ K. The agreement becomes worse for the higher temperatures due to a disagreement in background collision strengths. This may be caused by partial wave convergence and differences in target state wave functions. Overall, the comparison in Figure 6 can serve as an accuracy estimate for the available effective collision strengths of S III.

The effective collision strengths are presented over a wide range of temperatures suitable for use in astrophysical plasmas modeling. We tabulated effective collision strengths for all transitions between 198 fine-structure levels in Table 5 at 10

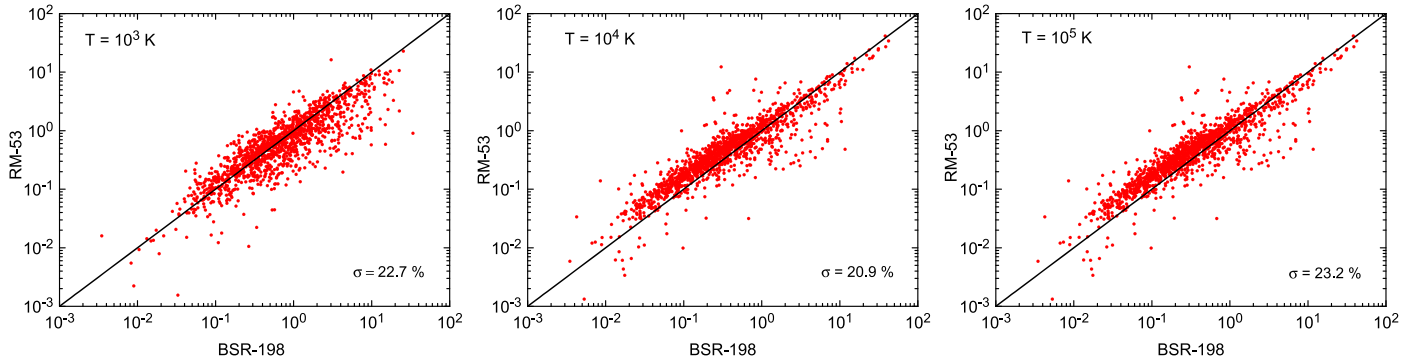

Figure 6. Comparison of effective collision strengths obtained in the present BSR-198 model with RM-53 model of Grieve et al. (2014) at electron temperatures (a) $T = 10^4$ K, (b) $T = 10^5$ K, and (c) $T = 10^6$ K. Also indicated in the panels is the average deviation, σ, from the BSR-198 results.

Table 5
Effective Collision Strengths for Fine-structure Transitions in S III

i–*k*	log *T*										
	3.0	3.2	3.4	3.6	3.8	4.0	4.2	4.4	4.6	4.8	5.0
1–2	1.61	1.65	1.69	1.80	1.94	2.01	1.98	1.87	1.74	1.57	1.36
1–3	1.49	1.36	1.25	1.19	1.16	1.18	1.24	1.31	1.35	1.32	1.21
1–4	6.85^{-1}	7.20^{-1}	7.46^{-1}	7.46^{-1}	7.29^{-1}	7.24^{-1}	7.36^{-1}	7.47^{-1}	7.38^{-1}	6.95^{-1}	6.15^{-1}
1–5	9.64^{-2}	1.09^{-1}	1.18^{-1}	1.23^{-1}	1.26^{-1}	1.29^{-1}	1.36^{-1}	1.44^{-1}	1.47^{-1}	1.38^{-1}	1.19^{-1}
1–6	1.85^{-1}	2.44^{-1}	3.31^{-1}	4.07^{-1}	4.40^{-1}	4.29^{-1}	3.96^{-1}	3.61^{-1}	3.29^{-1}	2.95^{-1}	2.53^{-1}
1–7	4.41^{-1}	4.35^{-1}	4.23^{-1}	4.06^{-1}	3.88^{-1}	3.72^{-1}	3.66^{-1}	3.71^{-1}	3.74^{-1}	3.67^{-1}	3.53^{-1}
1–8	3.97^{-1}	3.95^{-1}	3.88^{-1}	3.71^{-1}	3.49^{-1}	3.29^{-1}	3.18^{-1}	3.14^{-1}	3.03^{-1}	2.79^{-1}	2.44^{-1}

(This table is available in its entirety in machine-readable form.)

temperatures that cover a broad range from log $T = 3.0$ to 6.0. These results cover IR, optical, UV, and EUV emission lines for modeling of various types of astrophysical plasmas. The IR [S III] 18.7 and 33.5 μm lines have been observed in low-density planetary nebulae and are useful for electron density analyses. The FUV and EUV lines due to dipole-allowed $3s^23p^2\ {}^3P$–$3s3p^3\ {}^3P^o$, $3s^23p3d\ {}^3P^o$, $3s^23p3d\ {}^3D^o$, $3s^23p3d\ {}^3P^o$, $^3D^o$, $3s^23p4s\ {}^3P^o$, $^3D^o$, and $3s^23p4d\ {}^3P^o$, $^3D^o$ lines can be used for electron density estimates of the Io plasma torus and the solar and stellar transition regions. The indices of the lower and upper levels of transitions have been taken from Table 1. The accuracy of the collision strengths for transitions between levels with strong configuration and term mixing may crucially depend on the accuracy of the representation of these mixings. The entire contents of Table 5 have been published in machine-readable format with an associated ReadMe file.

4. Summary

The effective averaged collision strengths for all transitions among the 198 fine-structure levels of S III have been calculated in the present work. Systematic comparisons have been made with the other available calculations of radiative and collision data for S III to assess the accuracy of the available database. The calculations were performed with the advanced BSR code (Zatsarinny 2006), which employs the *R*-matrix method in the *B*-spline basis. The term-dependent orbital sets have been used to obtain a very accurate S III target states description. Both short-range and long-range correlation effects in the target states have been comprehensively included. The calculated excitation energies show very good agreement with the available experimental values for most levels considered in our work. The accuracy of collision rates is further improved using experimental thresholds in our collision calculation. The ordering of theoretical target energies agrees with the experiment, except for the $3s^23p4s\ {}^1P_1^o$ level. The effective collision strengths for many transitions are significantly enhanced because of the presence of resonances in the total collision strengths at low electron energies. There are significant discrepancies in the near-threshold energy region with other theories. We also presented a comparison of transition probabilities and lifetimes of excited levels to assess the accuracy of radiative data. Based on the accurate description of target states and more extensive close-coupling expansions, our results should be most accurate among the available calculations. The effective collision strengths are presented over a wide range of temperatures and should be useful for the analysis of various astrophysical plasmas.

This work was supported by the United States National Science Foundation under grant number AST-1714159 from the Astronomy and Astrophysics Program. The authors acknowledge Mr. E. Maroha for his assistance in generating some of the target wave functions. The numerical calculations were made possible by the XSEDE allocation under Grant No. PHY-170047.

References

Abou El-Maaref, A., Uosif, M. A. M., Allam, S. H., & El-Sherbin, T. M. 2012, ADNDT, 98, 589
Badnell, N. R. 2011, CoPhC, 182, 1528
Binette, L., Matadamas, R., Hagele, G. F., et al. 2012, A&A, 547, A29
Burke, P. G., Burke, V. M., & Dunseath, K. M. 1994, JPhB, 27, 5341
Curdt, W., Landi, E., & Feldman, U. 2004, A&A, 427, 1045
Feldman, P. D., Strobel, D. F., Moos, H. W., & Weaver, H. A. 2004, ApJ, 601, 583
Froese Fischer, C. 2007, CoPhC, 176, 559
Froese Fischer, C., Tachiev, G., & Irimia, A. 2006, ADNDT, 92, 607
Galaýs, M. E., Mendoza, C., & Zeippen, C. J. 1995, A&AS, 111, 347
Glass, R., & Hibbert, A. 1978, CoPhC, 16, 19
Grieve, M. F. R., Ramsbottom, C. A., Hudson, C. E., & Keenan, F. P. 2014, ApJ, 780, 110
Hall, D. T., Gladstone, G. R., Moos, H. W., et al. 1994, ApJL, 426, L51
Hibbert, A. 1975, CoPhC, 9, 141
Hudson, C. E., Ramsbottom, C. A., & Scott, P. J. 2012, ApJ, 750, 65
Johansson, A. E., Magnusson, C. E., Joelsson, I., & Zetterberg, P. O. 1992, PhyS, 46, 221
Mendoza, C., & Bautista, M. A. 2014, ApJ, 785, 91
Nicholls, D. C., Dopita, M. A., Sutherland, R. S., Kewley, L. J., & Palay, E. 2013, ApJS, 207, 21
Rubin, R. H., Simpson, J. P., Colgan, S. W. J., et al. 2008, MNRAS, 387, 45
Spinoglio, L., Pereira-Santaella, M., Dasyra, K. M., et al. 2015, ApJ, 799, 21
Tayal, S. S. 1997a, ApJ, 481, 550
Tayal, S. S. 1997b, ADNDT, 67, 331
Tayal, S. S., & Gupta, G. P. 1999, ApJ, 526, 544
Tayal, S. S., & Zatsarinny, O. 2011, ApJ, 743, 206
Tayal, S. S., & Zatsarinny, O. 2014, ApJ, 788, 24
Zatsarinny, O. 2006, CoPhC, 174, 273
Zatsarinny, O., & Froese Fischer, C. 2000, CoPhC, 124, 247